Effects of viscosity ratio and three dimensional positioning on hydrodynamic interactions between two viscous drops in a shear flow at finite inertia

Rajesh Kumar Singh and Kausik Sarkar[a)]
Department of Mechanical Engineering, University of Delaware, Newark, Delaware 19716, USA

(Received 14 July 2009; accepted 30 September 2009; published online 26 October 2009)

Drops driven toward each other by shear at finite inertia follow two distinct types of trajectories. Type I trajectory is similar to the one in Stokes flow where drops slide past each other. However, at finite inertia, drops display a new type II trajectory, where they reverse their paths. Increasing viscosity ratio results in a transition from type II to type I trajectory. The transition is caused by decreased drop deformation and increased alignment with the flow at higher drop viscosity; both decrease the zone of reversed streamlines that accompanies a drop at finite inertia. The transition is delineated in a phase diagram of Reynolds number and viscosity ratio for different capillary numbers. The critical viscosity ratio, where a type II transitions into type I, increases with Reynolds number except at higher capillary numbers, where the critical viscosity ratio shows a slight nonmonotonic variation with Reynolds number. Also, it is nonmonotonic with capillary numbers in that for a fixed Reynolds number, the critical viscosity ratio first increases with increasing capillary number and then decreases. Similar to the Stokes regime, increased viscosity ratio leads to a decreased postcollision cross-stream separation effectively decreasing the shear induced diffusion. Higher viscosity ratio results in an increased separation between drops during encounter, which results in a smaller interaction time. With drops placed initially at different shear planes, drops come under the influence of the reversed flow zone around a single drop that broadens off the central shear plane. Consequently, the trajectory changes from type I to type II as the offset in the vorticity direction increases. The change depends on the initial offset in the shear direction as well. The final displacement in the shear direction varies linearly with the initial offset. The net relative displacement in the shear direction shows a gradual decrease with increasing offset. The net relative displacement in the vorticity direction with increasing offset first increases from a zero value when drops are placed at the same shear plane to a maximum and then decreases. For certain cases, it reaches a negative value. © *2009 American Institute of Physics*. [doi:10.1063/1.3253351]

I. INTRODUCTION

The interactions between particles or drops dictate the overall behavior of a nondilute suspension or emulsion. Pairwise interactions completely determine the rheology to $O(c^2)$, where c is the concentration of the dispersed phase.[1] For dense suspensions, where multiparticle interactions become important, pair interaction is still the fundamental building block—high fidelity expressions of pairwise mobility and resistance functions[2,3] between spheres at varying separation are critical to Stokesian dynamics code for suspensions of rigid spheres.[4–6] Stokesian dynamics for rigid suspensions and boundary element methods for emulsions have been used very effectively in exploring the rheology at the Stokes limit.[5,7–13] In contrast, the effects of inertia on suspensions and emulsions remain relatively unexplored. We have recently performed a numerical investigation of pairwise interactions between deformable drops in shear at finite inertia.[14] It was restricted to viscosity matched systems and for drops initially placed in the same shear plane. In this paper, we study the effects of viscosity ratio and arbitrary initial positioning of the drop pair in different shear planes.

Recent investigations by our group showed that small amount of inertia can have significant effects on the behavior of a single drop[15–19] and, consequently, on the rheology of an emulsion including changes in the sign of the first and second normal stresses.[20–22] Concurrently, other groups found strong effects of inertia on flows around a freely rotating particle—the closed streamlines seen in Stokes flow disappear, giving rise to spiraling and reversed streamlines, leading to enhanced heat transfer at finite Peclet numbers.[23–25] Consequently, a particle pair shows reversed and spiraling trajectories and irreversible cross-stream migration in the presence of inertia.[26] In our recent study on drop pairs, we found that the drops show two distinct types of trajectory—drops passing each other similar to those seen in Stokes flow (type I) and drops reversing their trajectories upon coming together (type II). The latter one is caused by the reversed streamlines around a single drop in shear.[14] However, drop deformability introduces further richness in behavior, in that while at low and high capillary numbers drops traverse type I trajectory, at intermediate capillary numbers, they follow type II. The phenomenon was explained by noting that with increasing capillary number, while increased drop deformation impedes sliding motion (favoring type II), increased

[a)]Telephone: (302)-831-0149. Electronic mail: sarkar@udel.edu.

drop alignment, flexibility and lesser interfacial stress favor type I. We note that a recent study investigates the effects of particle inertia (finite Stokes number), albeit in a Stokes flow, on the collision trajectory between drop pairs driven together by a shear or a pure straining motion.[27] However, due to the lack of inertia in the underlying flow, drops traverse only type I trajectory in shear.

In Stokes flow regime, drop dynamics is determined by viscosity ratio λ along with the capillary number.[28,29] Drops deform less at low capillary numbers due to interfacial tension forces dominating the viscous stretching and at high viscosity ratios when a strong circulating flow inside impedes stretching. The critical capillary number for breakup tends to have a maximum around $\lambda \sim 1$, increasing both for lower and higher viscosity ratios. Unlike in an extensional flow, drop breakup in shear is not possible above a viscosity ratio even for arbitrarily large shear rate. Apart from lesser deformation, a drop aligns more with the flow at high viscosity ratios. These phenomena in single drop dynamics anticipate significant effects of viscosity ratio on pair dynamics. Indeed, previous two and three dimensional boundary element simulations of pairwise interactions between deforming drops demonstrate that viscosity ratio strongly affects drop collisions and migration, resulting, for instance, in decreased hydrodynamic diffusivity at increased viscosity ratios.[10–13]

As for initial drop positioning, Loewenberg and Hinch,[12] while computing drop migration and resultant self-diffusivity, found them to be higher in the gradient direction compared to the vorticity direction, illustrating the three dimensional nature of the interaction. Similar three dimensional effects were also investigated for pair interactions between capsules enclosed by elastic neo-Hookean membrane by Lac and Barthes-Biesel using boundary element simulation.[30] Following up their earlier study of capsules being in the same shear plane,[31] in this work they found that an offset in the vorticity direction results in the negative displacement for capsules in contrast to the case of drops. For rigid particle pairs, Kulkarni and Morris found spiraling trajectories with nonzero offset in the vorticity direction at finite inertia.[26]

Viscosity ratio and three dimensional positioning are shown below to generate an unusually rich spectrum of behaviors to merit careful consideration. Similar to our previous study, front tracking method is used for the simulation. The mathematical formulation and its numerical implementation are described in Sec. II. We study the effect of viscosity ratio and initial drop configuration in the vorticity direction in detail in Sec. III. In Sec. IV, we summarize the present work.

II. GOVERNING EQUATIONS AND NUMERICAL IMPLEMENTATIONS

We use front tracking finite difference method to simulate the motion and deformation of the drops. The method has been described in detail previously[16,18,32–35] and only a brief sketch is provided here. The governing equations are

$$\nabla \cdot \mathbf{u} = 0, \tag{1}$$

$$\frac{\partial(\rho \mathbf{u})}{\partial t} + \nabla \cdot (\rho \mathbf{u}\mathbf{u}) = -\nabla p + \nabla \cdot [\mu \nabla \mathbf{u} + (\mu \nabla \mathbf{u})^T] - \int_{\partial B} d\mathbf{x}_B \kappa \mathbf{n} \Gamma \delta(\mathbf{x} - \mathbf{x}_B), \tag{2}$$

where p is the pressure, ρ is the density, μ is the viscosity, and Γ is the interfacial tension. The density and viscosity are uniform in each phase. ∂B is the surface of the drop consisting of points $\mathbf{x}_B$. κ is the local curvature and $\mathbf{n}$ is the outward unit normal vector to ∂B. $\delta(\mathbf{x}-\mathbf{x}')$ is the three dimensional Dirac-delta function. The interfacial tension force expressed as a singular body force in Eq. (2) is distributed smoothly around the interface using a mollified representation of the delta function. The two phase drop-matrix system with different properties across the sharp interface is also transformed into a single-fluid formulation using a smoothly varying representation of the properties. The resultant equation is solved on a uniform staggered grid using a fractional time-stepping finite difference method. The front interface is discretized using triangular elements. The discretized front is used for determining the properties and the surface force. The drop motion is described by moving the front nodes by the locally interpolated velocities. An adaptive front regridding scheme is used to prevent excessive distortion of the front elements. The explicit scheme suffers from the restriction on time steps at low Reynolds number $[\Delta t < 0.25(\Delta x)^2 \rho/\mu]$. To overcome this restriction, we treat some of the diffusive terms implicitly in alternate spatial direction (ADI). The ADI scheme reduces the time step by one order of magnitude.[18] We also adhere to other criteria $\Delta t < 2.0\mu/(\rho U_{\max}^2)$ and $\Delta t < \Delta x/U_{\max}$ at high Reynolds numbers to ensure overall convergence of our simulation.

Two equal-size spherical drops with undeformed radius a are placed symmetrically in the computational domain. (Note that a change in the frame would result in symmetric configuration for drops not placed symmetrically.[14]) A periodic boundary condition is imposed in the flow (x) and the vorticity (z) directions. The top and the bottom walls of the domain move in the opposite directions with velocity $\boldsymbol{U}$ and $-\boldsymbol{U}$, respectively, resulting in a simple shear (with rate $\dot{\gamma}$ in the y-direction). We use a domain size of $30a \times 10a \times 5a$ for cases when both drops are in the same shear plane with a discretization level of $288 \times 96 \times 48$. For cases with drops initially separated in the vorticity direction, a domain size of $30a \times 10a \times 10a$ is used with discretization level of $288 \times 96 \times 96$. In our previous article, grid convergence and the domain size dependence have been carefully investigated for drops in the same vorticity plane to show that the domain sizes in the flow and the gradient directions are sufficient.[14] Note that confinement in the gradient direction has been shown to lead to reversed trajectories even in a Stokes flow.[36] We found that for the range of Reynolds number considered here, the flow is not altered when the domain size is further increased, but a smaller domain size leads to a change in the trajectory type. Below, we investigate domain-size dependence for drops with an initial offset in the vorticity

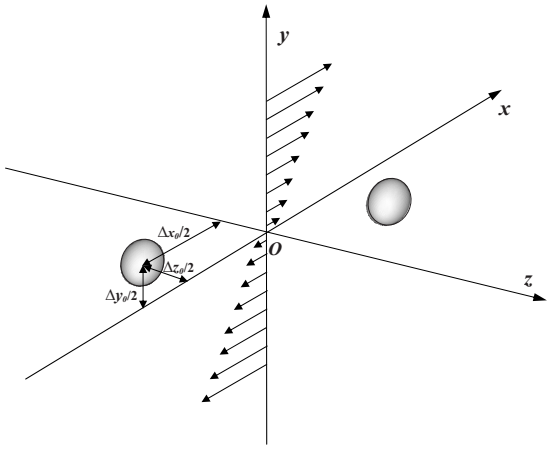

FIG. 1. Schematic layout of two drops in a shear flow showing the initial positions of the drops and imposed shear in the y-direction.

direction. Figure 1 shows a three dimensional view of the computational flow domain. We use the radius of undeformed drop a as the length scale and the inverse shear rate $\dot{\gamma}^{-1}$ as the time scale to define various dimensionless parameters for the problem: Reynolds number $\mathrm{Re}=\rho_m \dot{\gamma} a^2/\mu_m$, capillary number $\mathrm{Ca}=\mu_m \dot{\gamma} a/\Gamma$, viscosity ratio $\lambda=\mu_d/\mu_m$, density ratio $\lambda_\rho=\rho_d/\rho_m$ (=1 here), and initial configuration parameters $\Delta x_0/a$, $\Delta y_0/a$, and $\Delta z_0/a$. Subscripts m and d stands for matrix and drops, respectively.

III. RESULTS AND DISCUSSIONS

In our previous paper,[14] our simulation was compared to the experimental observations by Guido and Simeone[37] of binary collision between polydimethylsiloxane drops in polyisobutylene matrix at vanishing Reynolds numbers for $\lambda=1.4$. The simulation showed excellent match for the evolution of deformation, inclination angle, angle of the line joining the drops, and their relative trajectory. In that paper, we studied the effects of inertia, capillary number variations, as well as $\Delta x_0/a$ and $\Delta y_0/a$ variations. We found that the drops change their trajectory at finite inertia. In Stokes flow, drops press against each other in the compressional quadrant, rotate together as a doublet, and then peel away from each other in the extensional quadrant. Unlike rigid spheres, drops show a net irreversible postcollision increase in the lateral (shear direction) separation due to the asymmetry in the approach and separation phases of the interaction.[11,12] With increasing inertia, we saw that the drops undergo a change in trajectory from this type I to a reversed type (type II). Here, we concentrate on the effects of viscosity ratio and $\Delta z_0/a$ variations on these two trajectories. Note that we use Taylor deformation measure $D=(L-B)/(L+B)$, where L and B are the maximum and the minimum distances of the drop interface from the center.[38] Because the problem involves many defining parameters, in the interest of brevity, we use a set of reference values for some of the parameters: unless stated otherwise explicitly, we keep $\Delta x_0/a=2.5$, $\Delta y_0/a=0.25$, $\Delta z_0/a=0$, $\mathrm{Ca}=0.2$, and $\mathrm{Re}=2$.

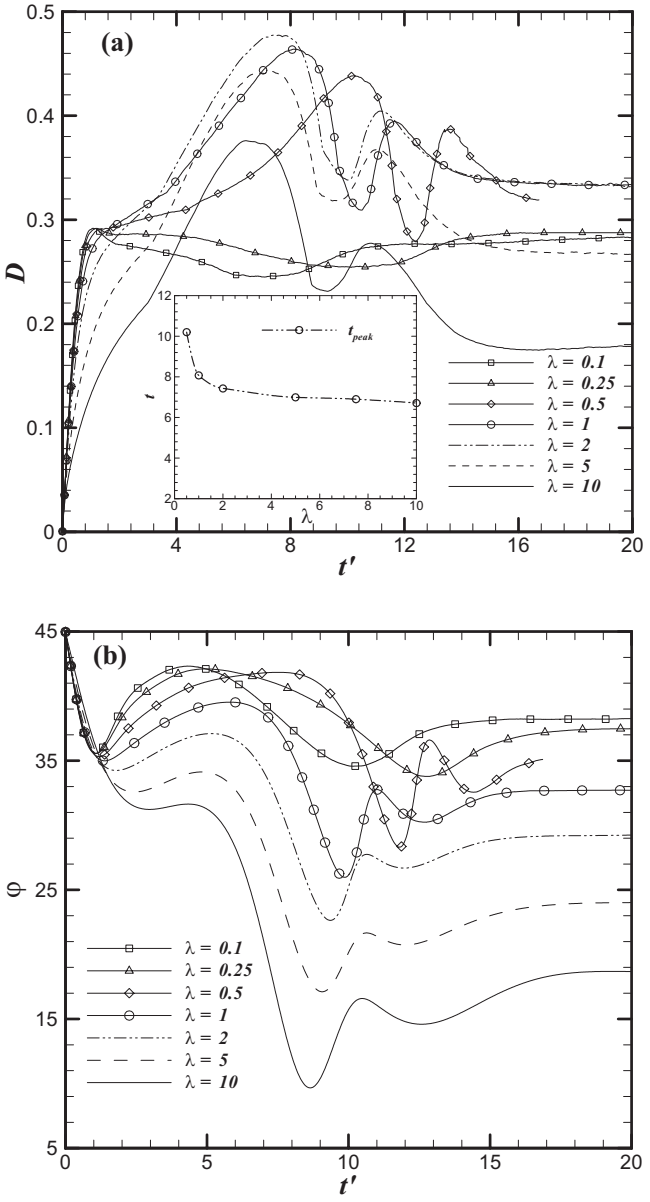

FIG. 2. Time history of (a) deformation and (b) orientation angle of the drops at $\mathrm{Re}=2$, $\mathrm{Ca}=0.2$, $\Delta x_0/a=2.5$, $\Delta y_0/a=0.25$, and different λ. The inset in (a) plots the time to reach peak deformation for type I trajectory.

A. Effects of viscosity ratio λ

In Fig. 2, we investigate the evolution of deformation [Fig. 2(a)] and inclination [Fig. 2(b)] for increasing viscosity ratio. For higher viscosity ratio ($\lambda \geqslant 0.5$), we see drop deformation characteristic of type I trajectory with two peaks, the first one corresponding to drops pressed in their compressional quadrant and the second, when they peel away in the extensional quadrant.[14] However, for lower λ, we see type II trajectories without any distinctive peak. Figure 3 clearly shows a type II trajectory for the lowest two values of viscosity ratio and type I for the others. Type II trajectory results from the region of reversed streamlines that appears near a drop[14] in a shear flow at finite inertia (Fig. 4). Each drop coming into the reversed streamline zone induced by the other is forced to traverse a reversed trajectory. For a single drop in shear, increasing viscosity ratio results in pro-

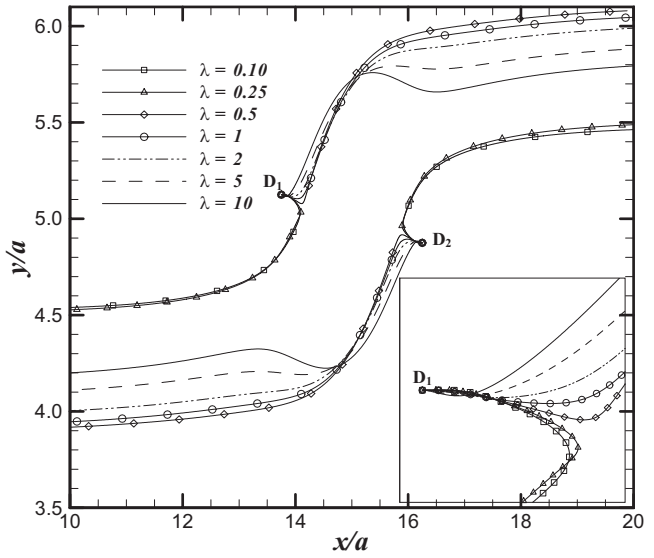

FIG. 3. Trajectories of the center of mass of the drops at Re=2, Ca=0.2, $\Delta x_0/a=2.5$, $\Delta y_0/a=0.25$ for different λ. D_1 and D_2 are the initial drop centers. The inset shows the magnified view of the left drop's trajectory at the beginning of drop interaction.

gressive alignment of the drops with the flow direction;[28] this facilitates drops flowing past each other in a type I trajectory. In Fig. 4, the flow around a single drop in shear at Ca=0.2 and Re=2 shows increased alignment of the deformed drop axis with the flow as the viscosity ratio increases. A resultant decrease in the size of the zone of reversed streamline further aids the transition from type II to type I. Also note the marked reduction in deformation with increasing viscosity ratio, which also lessens the hindrance to drops passing by each other in type I trajectory.

A closer observation of Fig. 2(a) reveals that the sudden steep rise in deformation that marks the onset of drops' alignment with each other in the compressional quadrant starts at later times for higher viscosity ratios, which can be ascribed to a slower response of high viscosity drops. Figure 2(b) also shows that the first minimum in inclination angle accompanying the onset of drop alignment occurs later at higher viscosity ratio. Also note (in the inset of Fig. 3) that higher viscosity ratio drops separate earlier in the gradient direction, whereas for lower viscosity ratios, drops move closer in the flow direction before they separate in the gradient direction. Separation in the gradient direction delays the onset of close interaction at higher λ. However, this separation also increases drop's relative velocity, which quickens the relative drop motion for higher viscosity ratios. Indeed, for cases undergoing type I trajectory, the time to reach the first maximum in deformation (when the drops are completely aligned in the compressional quadrant) decreases with viscosity ratio [inset in Fig. 2(a)]. Later, when the drops are sliding over each other, the deformation shows a minimum and then a second maximum when they peel away in the extensional quadrant. From the onset of deformation to the second minimum defines the interaction cycle. Although the interaction starts later, the interaction time is shorter for high viscosity ratio cases because of the higher relative velocity mentioned above.

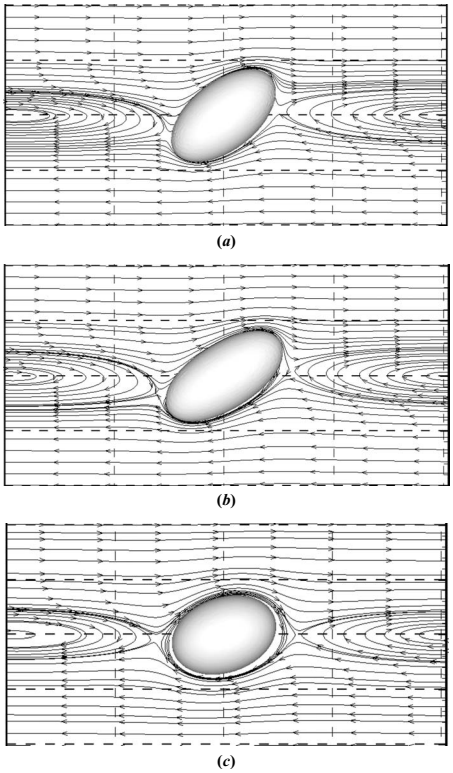

FIG. 4. Streamline plots at the central shear plane for a single drop at Re=2 and Ca=0.20 for (a) λ=0.1, (b) λ=1.0, and (c) λ=10.

For a single drop in shear, the drop deformation is maximum around $\lambda \sim 1$, reducing for both decreasing and increasing viscosity ratios.[28,39] We see a similar effect of viscosity ratio on the deformation of the interacting drops [Fig. 2(a)]. The maximum deformation increases until $\lambda \leqslant 2$ with increasing viscosity ratio. For $\lambda > 2$, it decreases. Plotting deformation and inclination as functions of $\Delta x/a$ instead of t' would show similar evolution for all parameters undergoing the same type of trajectory (not shown here for brevity).[14] Figure 5 shows drop interactions at six time instants for three different viscosity ratios λ=0.1, 1.0, and 10. For the first value, the drops traverse a type II trajectory, while for the other two, a type I trajectory. We also note that for λ=10, drops peel away quicker. Also note that the film thickness at the closest approach is higher at higher viscosity ratios as was also seen by Loewenberg and Hinch[12] for $2 \leqslant \lambda \leqslant 8$ and $\mathrm{Ca}=O(1)$.

For type I trajectories in Fig. 3, we note that postcollision drops experience a net cross-stream displacement in contrast to the reversible rigid particle-pair trajectory in a Stokes flow. This displacement results in the shear induced diffusion. Because with increasing viscosity ratio, drops behave more like rigid particles, they show increasing tendency to revert to their precollision streamlines, resulting in a reduced self-diffusion. Figures 6(a) and 6(b) show the evolution of streamwise and cross-stream separations between drops. The streamwise separation $\Delta x/a$ increases steeply after collision for type I trajectory, whereas for type II trajectory (λ=0.1,0.25), it becomes negative. With increasing viscosity ratio, $\Delta x/a$ starts increasing earlier, giving rise to a

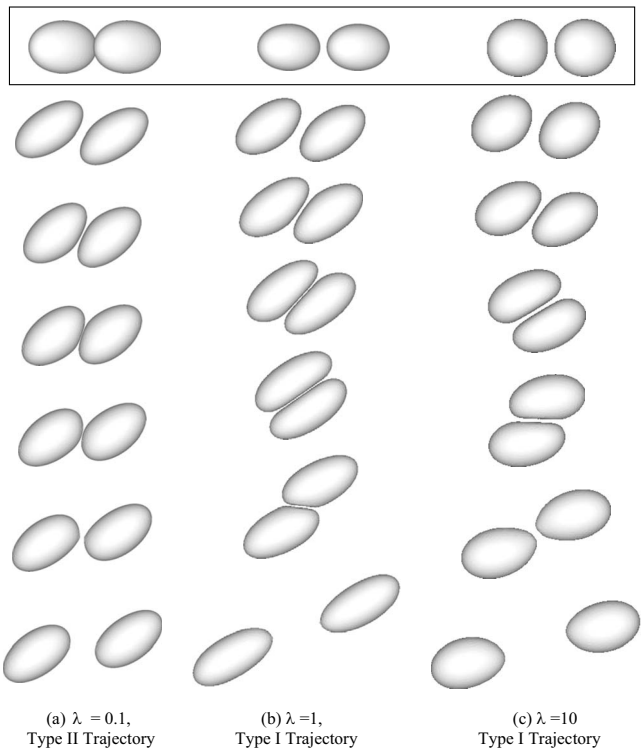

FIG. 5. Images of drops at $t'=2$, 4, 7, 9, 11, and 13 for Ca=0.2, Re=2, $\Delta x_0/a=2.5$, $\Delta y_0/a=0.25$, and three viscosity ratios showing two types of trajectories. Drop's shape in the top box shows their projection in the $y=0$ plane at $t'=2$.

higher value. We already noted that the drops start their cross-stream separation earlier with increasing viscosity ratio, which increases their relative streamwise motion resulting in higher $\Delta x/a$. However, after collision, more viscous drops tend to revert back to their precollision streamlines. Consequently, they experience smaller streamwise velocity, and $\Delta x/a$ for high viscosity drops ultimately becomes smaller than those for lower viscosity drops.

The cross-stream separation in Fig. 6(b) shows that the final cross-stream offset decreases with increasing viscosity ratio (shown also in the inset) for type I trajectory. However, if one compares it with the Stokes flow case (Fig. 7 in Ref. 12), one notes that the offset is larger at finite inertia, and its decrease with viscosity ratio is not as sharp. In Fig. 7, cross-stream separation for Re=0.1 further elucidates this. We see only type I trajectory for all viscosity ratios (for the lowest value λ=0.1, we see a slight reversing trend initially but finally a type I trajectory) at this reduced Reynolds number. This demonstrates that whether there is a transition from one type of trajectory to the other and the critical $\lambda(\lambda_{cr})$ for transition depends on the Reynolds number. As we noted previously, this transition also depends sensitively on the capillary number and initial offsets.[14]

In Fig. 8, we explore the transition of trajectories in a phase diagram in the Re-λ space for $\Delta x_0/a=2.5$, $\Delta y_0/a=0.25$, and $\Delta z_0/a=0$. Using an extensive set of simulations, we delineate the regions for the two types of trajectories [Fig. 8(a) shows this for Ca=0.2]. We note that below Re ~0.4, drops experience type I trajectory for all λ examined ($\lambda \geqslant 0.01$). Increasing Reynolds number increases the zone

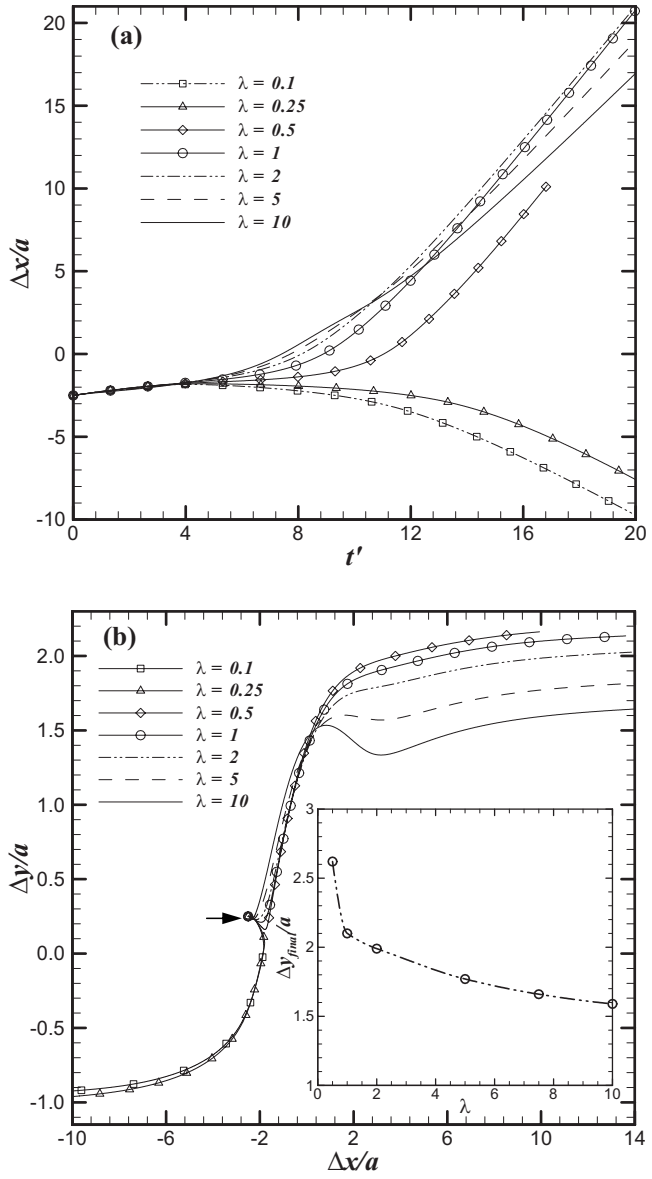

FIG. 6. (a) $\Delta x/a$ with t' and (b) $\Delta y/a$ with $\Delta x/a$ for Ca=0.2, Re=2, $\Delta x_0/a=2.5$, $\Delta y_0/a=0.25$ at various viscosity ratios. The arrow indicates the initial position. The inset in (b) shows the variation in the final value of $\Delta y/a$ with λ for type I trajectory.

of reversed streamlines and therefore increases the tendency toward type II,[14] as can be seen in this diagram. Finding exact value of the critical viscosity ratio λ_{cr} that marks the transition is difficult, as near the transition results might sensitively depend on specifics of the numerical implementation. In Fig. 8(a), we show the simulations used to demonstrate the two different regions. We believe that it captures the transition between the two types and roughly delineates the critical viscosity ratio curve. λ_{cr} shows a slight nonmonotonicity with Reynolds number at this moderately large value of capillary number (Ca=0.2) at the high Re end of the diagram. The drop shapes at the same time instant for two Reynolds numbers at the same viscosity ratio (λ=0.45) in the inset of Fig. 8(a) show that due to a slightly higher deformation, the drops at Re=6 [inset (ii)] traverse type I trajectory with increased alignment with the flow, while at Re=5 [inset (i)], they reverse their trajectories.

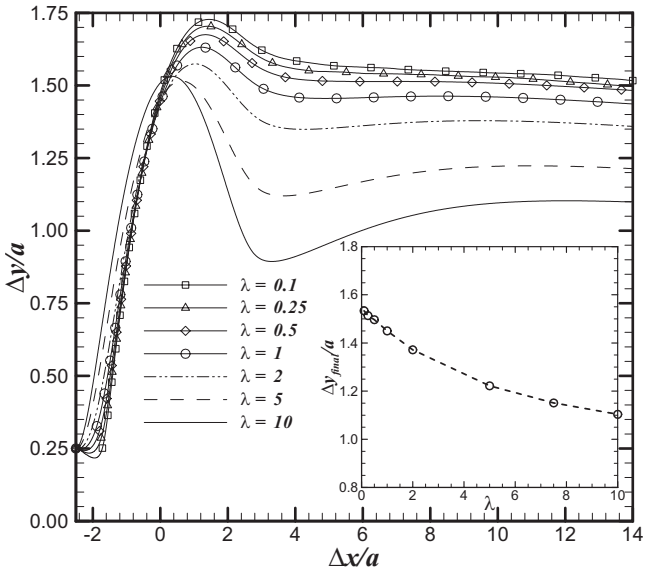

FIG. 7. Relative trajectories of drops at Re=0.1, Ca=0.2, $\Delta x_0/a=2.5$, $\Delta y_0/a=0.25$, and various viscosity ratios. The inset in (b) shows the final value of $\Delta y/a$ as a function of λ.

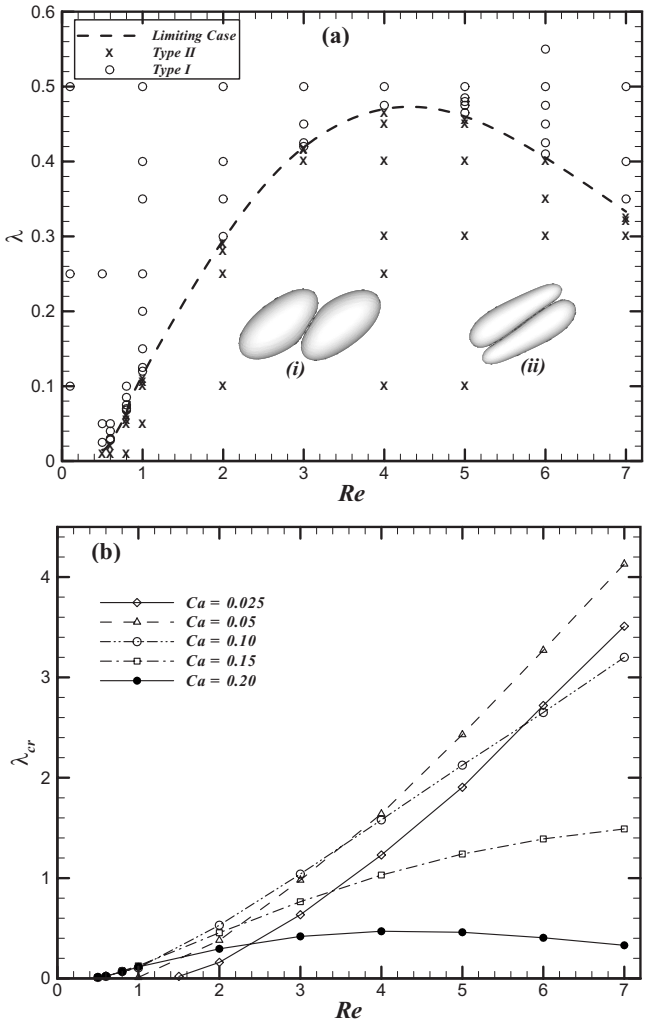

FIG. 8. (a) Types of trajectory as a function of Re and λ for Ca=0.2, $\Delta x_0/a=2.5$, and $\Delta y_0/a=0.25$. Drop's shapes for λ=0.45 at $t'=14$ for (i) Re=5 and (ii) Re=6 in the inset. (b) Variation in λ_{cr} as a function of Re for different Ca values with the same initial offset.

In Fig. 8(b), we show λ_{cr} as a function of Re for different capillary numbers. Each curve is produced with progressively refined simulations around the critical value of viscosity ratio similar to what was shown in Fig. 8(a). We notice that the slight nonmonotonicity at high Re for Ca=0.2 is absent for lower Ca values. It further substantiates the argument that the reduction at the high Re end (at Ca=0.2) is due to increased alignment with the flow of a highly deformed drop. In fact, at smaller capillary numbers, λ_{cr} increases linearly with Reynolds number at the high Re end. In Ref. 14, we found a nonmonotonic variation with Ca for λ=1—type I trajectory for low and high Ca and type II for intermediate Ca due to the competition between increased deformation favoring type II and increased drop alignment favoring type I. We see a similar behavior here in Fig. 8(b)—λ_{cr} curve for Ca=0.05 is higher than both a lower Ca=0.025 and a higher Ca=0.1 for Re>4. Compared to Ref. 14, here a more complete picture emerges, extending to cases of $\lambda \neq 1$.

B. Effects of initial separation $\Delta z_0/a$

So far in this work and in our previous study,[14] we restricted to cases without any initial separation in the vorticity direction, $\Delta z_0/a=0$. Lac and Barthes-Biesel[30] found that a full three dimensional initial positioning with a nonzero offset in the vorticity direction gives rise to a negative displacement for a pair of capsules in free shear. For rigid particle pairs, Kulkarni and Morris found spiraling trajectories at finite inertia with $\Delta z_0/a \neq 0$.[26] Here, we investigate the effect of nonzero $\Delta z_0/a$ on drop interactions. For brevity, we restrict this study to viscosity matched system; simulation showed that the effect of viscosity ratio for $\Delta z_0/a \neq 0$ remains similar to the previous section—increasing viscosity ratio favors a change from type II to type I trajectory. For the same reason, we also restrict ourselves to the Re=2 case, but note that for Re=0.1, we see type I trajectory for all $\Delta z_0/a$ (not shown here). We have investigated in detail the effects of computational domain size in the x- and y-directions in our previous study[14] when both drops are in the same shear plane. Figure 9 shows the effect of domain size in the z-direction for both types of trajectory (type II in the inset) with type I having two peaks in deformation and no discernible peak for type II. For $\Delta z_0/a \neq 0$, expectedly one needs a longer domain in the z-direction; $30a \times 10a \times 10a$ size suffices for cases with $\Delta z_0/a \sim 1.0$.

We note from Fig. 9 that increasing $\Delta z_0/a$ changes trajectory from type I to type II with other parameters unchanged at finite inertia. In Fig. 10, we systematically vary $\Delta z_0/a$ from zero to 2.0 and plot the relative trajectories $\Delta x/a$, $\Delta y/a$, and $\Delta z/a$ between the drops. Comparison of Figs. 3 and 6(b) shows that the relative trajectory closely mirrors the trajectory of one of the drops; therefore, here we show only the relative trajectory. Figure 10 shows that $\Delta z_0/a \geq 0.5$ results in transition from type I (increasing $\Delta y/a$ with time) to type II (decreasing $\Delta y/a$ with time) trajectory. This can be explained by noticing the three dimensional flow field around a single drop; we show two dimensional slices of the flow field at different z-planes in Fig. 11. Note that the

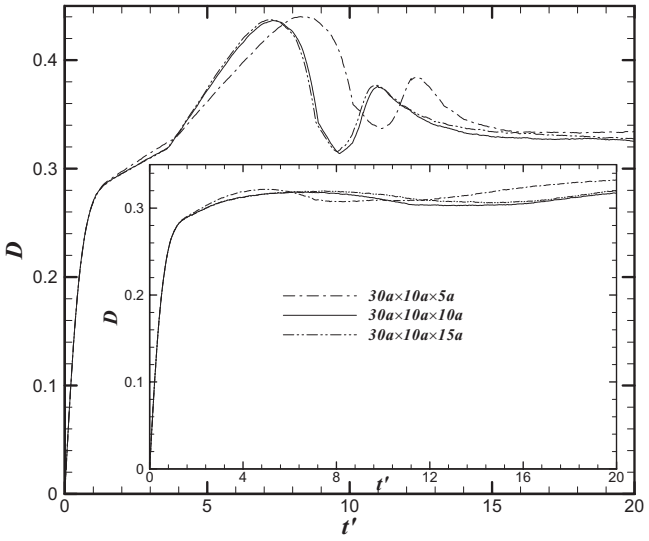

FIG. 9. Deformation vs time at Ca=0.2, Re=2, $\Delta x_0/a=2.50$, $\Delta y_0/a=0.25$, and $\Delta z_0/a=0.25$ (type I trajectory) for three computational domain sizes. The inset in the figure shows the same plot for type II trajectory for $\Delta z_0/a=1.0$ and the same values of other parameters.

zones of reversed streamlines fore and aft of the drop appearing at finite inertia approach each other closer to the central $x=0$ plane for increasing z leading to a saddle point. Consequently, the overlap of the other drop with the reversed zone increases with increasing $\Delta z_0/a$, resulting in a transition from type I to type II. Note that a similar three dimensional flow field at finite inertia is found around a free rigid sphere in shear.[23,24] However, for rigid particles, away from the sphere in the z-direction, a zone of circular spiraling streamlines appears, which is absent in the case of a deformable drop. Consequently, we do not see any spiraling trajectories seen for a pair of rigid spheres.[26] However, for cases with very high λ, which are closer to a solid sphere, we see spiraling streamlines (not shown here).

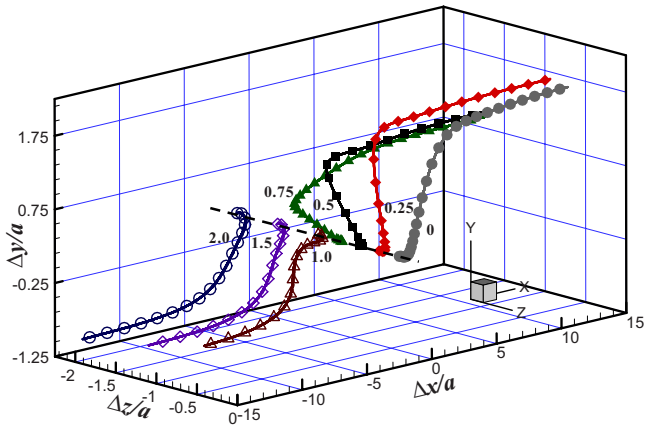

FIG. 10. (Color online) Three dimensional relative trajectory of the two interacting drops at Ca=0.2, Re=2, $\Delta x_0/a=2.5$, $\Delta y_0/a=0.25$, and various $\Delta z_0/a$. Gray filled circle: $\Delta z_0/a=0$; (red) filled diamond: $\Delta z_0/a=0.25$; (black) filled rectangle: $\Delta z_0/a=0.5$; (green) filled delta: $\Delta z_0/a=0.75$; (brown) unfilled triangle: $\Delta z_0/a=1$; (violet) unfilled diamond: $\Delta z_0/a=1.5$; and (blue) unfilled circle: $\Delta z_0/a=2$. Symbols on the dashed line indicate the initial position.

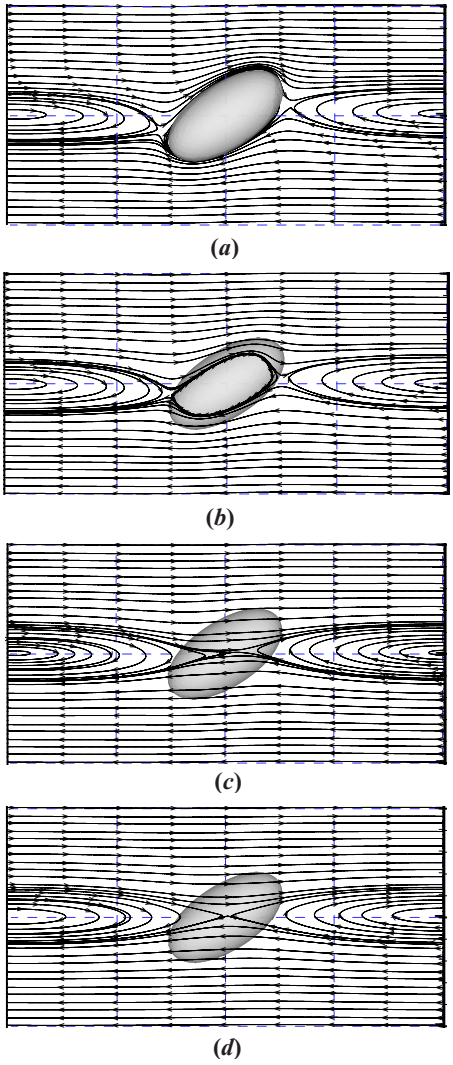

FIG. 11. (Color online) Streamlines at different z-planes of the flow domain for a single drop at Re=2 and Ca=0.2; (a) $z/a=0$, (b) $z/a=0.5$, (c) $z/a=1$, and (d) $z/a=1.5$.

In Figs. 12(a) and 12(b) we plot $\Delta y/a$ and $\Delta z/a$ to show quantitatively how $\Delta z_0/a$ affects displacements in the gradient and vorticity directions. We notice that increasing $\Delta z_0/a$ decreases $\Delta y/a$ because the interaction between drops decreases. The inset in Fig. 12(a) shows that the final value varies almost linearly with $\Delta z_0/a$ for type I trajectory. In contrast, type II trajectory ($\Delta z_0/a \geq 1.0$) is not affected much by $\Delta z_0/a$. The in-plane initial positioning ($\Delta z_0/a=0$) results in drops remaining in the same shear plane due to symmetry [Fig. 12(b)]. Increasing $\Delta z_0/a$ increases $\Delta z/a$—i.e., drops move further away from each other in the z-direction—for type I trajectory. For type II trajectories (at $\Delta z_0/a \geq 1.0$), increasing $\Delta z_0/a$ decreases net z-excursion of the trajectory.

For very large $\Delta z_0/a$, we expect the interaction to be too weak to cause any further shift in the z-direction. Therefore, a nonmonotonic behavior is expected. We also note that for higher values of $\Delta z_0/a$ when drops experience a type II trajectory, $\Delta z_{\text{final}}/a$ becomes less than $\Delta z_0/a$ [Fig. 12(b)], i.e., net displacement becomes negative. Lac and Barthes-Biesel[30] noted such a negative net displacement for

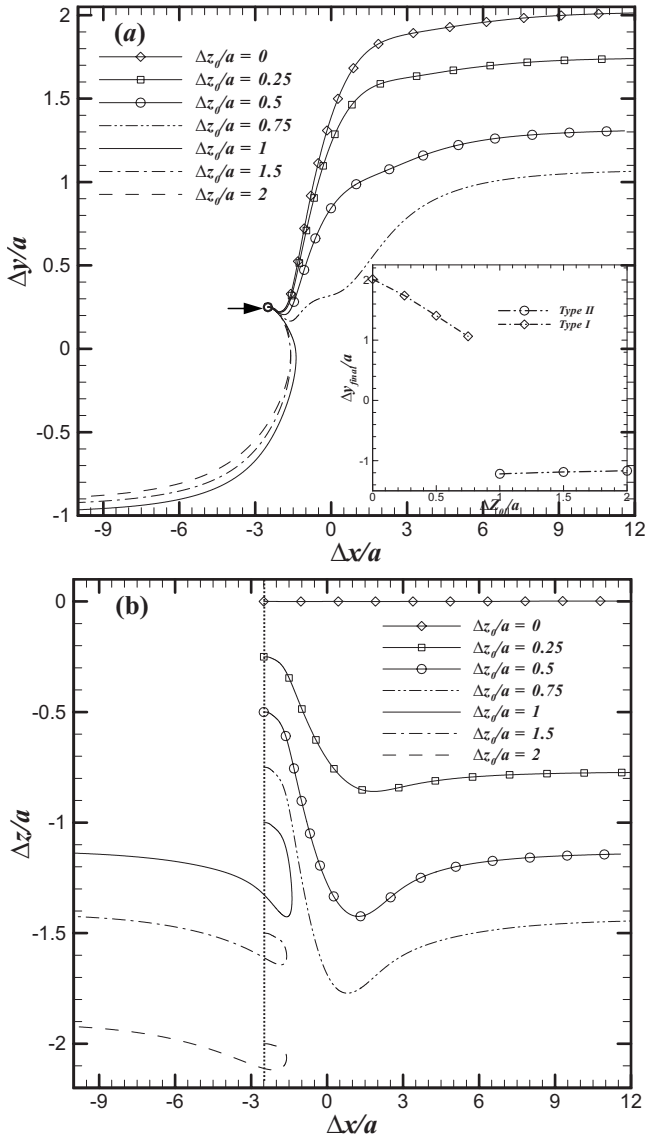

FIG. 12. Projections of the relative trajectories of two drops at the (a) x-y plane and (b) x-z plane for Re=2, Ca=0.20, $\Delta x_0/a$=2.5, $\Delta y_0/a$=0.25, and various $\Delta z_0/a$ values. The arrow in (a) and the points on the dotted line in (b) indicate the initial position. The inset in (a) shows the variation in the final value $\Delta y/a$ as a function of $\Delta z_0/a$.

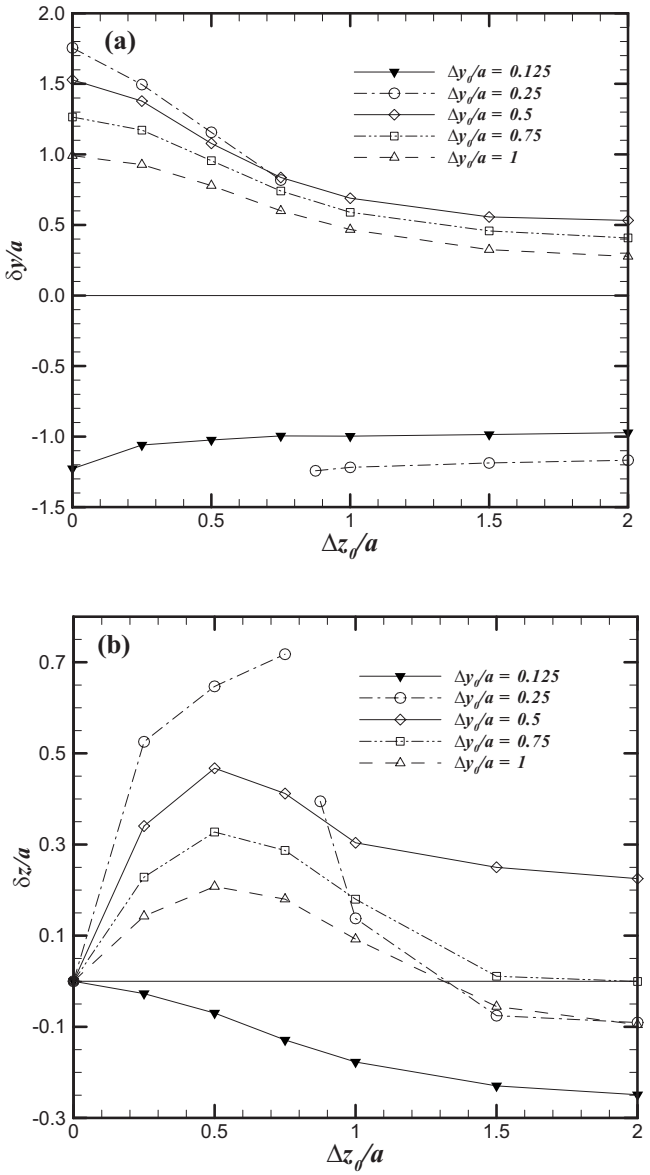

FIG. 13. The net relative displacement (a) $\delta y/a$ and (b) $\delta z/a$ as a function of $\Delta z_0/a$ for different $\Delta y_0/a$. Other values are the same as those in Fig. 12.

capsule pairs in a Stokes flow. We plot (as was also done in Ref. 30) net displacement $\delta y/a=(\Delta y_{\text{final}}-\Delta y_0)/a$ and $\delta z/a=(\Delta z_{\text{final}}-\Delta z_0)/a$ as functions of $\Delta z_0/a$ for varying $\Delta y_0/a$. Figure 13(a) shows that $\Delta y_0/a=0.125$ results in type II trajectory for all $\Delta z_0/a$, while for $\Delta y_0/a=0.25$, one sees type I trajectory for $\Delta z_0/a<0.8$, and type II otherwise. Other values of $\Delta y_0/a$ lead to type I for all $\Delta z_0/a$. $\delta y/a$ decreases with increasing $\Delta z_0/a$ as noted before, but does not change much with $\Delta y_0/a$ except when it causes a trajectory-type change in conformity with what was observed in our previous study.[14] For cases traversing type I trajectory, increasing $\Delta y_0/a$ expectedly decreases $\delta y/a$. On the other hand, as we anticipated above, $\delta z/a$ in Fig. 13(b) shows a nonmonotonic change with $\Delta z_0/a$. With increasing initial z-offset, it first increases from the zero value at the symmetry plane, but later it reduces when large initial z-separation decreases the interaction. In fact, for $\Delta y_0/a=1$, we get a slightly negative $\delta z/a$ for a type I trajectory, as was also observed for a pair of capsules.[30] Note that Subramanian and Brady found a negative net displacement in vorticity and gradient directions for a pair of rigid spheres in a shear when they accounted for particle inertia (finite Stokes number) in an otherwise Stokes flow.[40] For lower value of $\Delta y_0/a$, one gets type II trajectory accompanied by a negative offset in both vorticity and gradient directions.

IV. SUMMARY

Our previous investigation of pairwise interaction between drops at finite inertia is here extended to cases where viscosity of the dispersed phase differs from that of the matrix, and drops are initially placed in different shear planes. Increasing viscosity ratio changes drop trajectory from type II (reversed) at lower viscosity ratio to type I (passing). This can be explained as resulting from decreased drop deformation and increased drop alignment with the flow at higher

viscosity ratios, both aiding drops to pass by in a type I trajectory. We delineate the regions in the Re-λ space corresponding to the two types of trajectories for different capillary numbers. The critical λ shows a nonmonotonic trend—it first increases with increasing Ca and then decreases. Increased viscosity ratio decreases the overall interaction time between drops, as the drop separation and thereby relative velocity between them increases. It also results in a decreased final cross-stream separation between drops, which would lead to a reduced self-diffusivity.

Pair interactions between drops in two different shear planes are affected by the three dimensional flow field around a single drop in shear: the reversed flow domain approaches the $x=0$ plane away from the central x-y plane of the drop. Therefore, drop trajectory transitions from type I to type II as the z-offset increases. However, it also depends on the y-offset—at higher $\Delta y_0/a$, drops show only type I trajectory. Increasing this offset results in a linear decrease in the relative y-displacement for drops traversing type I trajectory. However, it displays a nonmonotonic behavior for the net relative displacement $\delta z/a$ in the vorticity direction. With increasing $\Delta z_0/a$, it first increases being pushed by the other drop and then decreases as their interaction decreases for very large separation. For some parameter values, it produces a negative final separation in the vorticity direction similar to what was observed for capsule pairs in a Stokes flow.

ACKNOWLEDGMENTS

K.S. acknowledges financial support from the NSF under Grant No. CBET-0625599.

[1] G. K. Batchelor and J. T. Green, "The determination of the bulk stress in a suspension of sphericalparticles to order c^2," J. Fluid Mech. **56**, 401 (1972).
[2] D. J. Jeffrey and Y. Onishi, "Calculation of the resistance and mobility functions for 2 unequal rigid spheres in low-Reynolds-number flow," J. Fluid Mech. **139**, 261 (1984).
[3] S. Kim and R. T. Mifflin, "The resistance and mobility functions of 2 equal spheres in low-Reynolds-number flow," Phys. Fluids **28**, 2033 (1985).
[4] G. Bossis and J. F. Brady, "Dynamic simulation of sheared suspensions. 1. general-method," J. Chem. Phys. **80**, 5141 (1984).
[5] J. F. Brady and G. Bossis, "Stokesian dynamics," Annu. Rev. Fluid Mech. **20**, 111 (1988).
[6] J. F. Brady, R. J. Phillips, J. C. Lester, and G. Bossis, "Dynamic simulation of hydrodynamically interacting suspensions," J. Fluid Mech. **195**, 257 (1988).
[7] G. Bossis, J. F. Brady, and C. Mathis, "Shear-induced structure in colloidal suspensions. 1. Numerical-simulation," J. Colloid Interface Sci. **126**, 1 (1988).
[8] A. Sierou and J. F. Brady, "Rheology and microstructure in concentrated noncolloidal suspensions," J. Rheol. **46**, 1031 (2002).
[9] T. N. Phung, J. F. Brady, and G. Bossis, "Stokesian dynamics simulation of Brownian suspensions," J. Fluid Mech. **313**, 181 (1996).
[10] R. Charles and C. Pozrikidis, "Significance of the dispersed-phase viscosity on the simple shear flow of suspensions of two-dimensional liquid drops," J. Fluid Mech. **365**, 205 (1998).
[11] X. F. Li, R. Charles, and C. Pozrikidis, "Simple shear flow of suspensions of liquid drops," J. Fluid Mech. **320**, 395 (1996).
[12] M. Loewenberg and E. J. Hinch, "Collision of two deformable drops in shear flow," J. Fluid Mech. **338**, 299 (1997).
[13] M. Loewenberg and E. J. Hinch, "Numerical simulation of a concentrated emulsion in shear flow," J. Fluid Mech. **321**, 395 (1996).
[14] P. O. Olapade, R. K. Singh, and K. Sarkar, "Pair-wise Interactions between deformable drops in free shear at finite inertia," Phys. Fluids **21**, 063302 (2009).
[15] K. Sarkar and W. R. Schowalter, "Deformation of a two-dimensional viscoelastic drop at non-zero Reynolds number in time-periodic extensional flows," J. Non-Newtonian Fluid Mech. **95**, 315 (2000).
[16] K. Sarkar and W. R. Schowalter, "Deformation of a two-dimensional drop at non-zero Reynolds number in time-periodic extensional flows: Numerical simulation," J. Fluid Mech. **436**, 177 (2001).
[17] K. Sarkar and W. R. Schowalter, "Deformation of a two-dimensional viscous drop in time-periodic extensional flows: Analytical treatment," J. Fluid Mech. **436**, 207 (2001).
[18] X. Y. Li and K. Sarkar, "Drop dynamics in an oscillating extensional flow at finite Reynolds numbers," Phys. Fluids **17**, 027103 (2005).
[19] X. Y. Li and K. Sarkar, "Drop deformation and breakup in a vortex at finite inertia," J. Fluid Mech. **564**, 1 (2006).
[20] X. Y. Li and K. Sarkar, "Numerical investigation of the rheology of a dilute emulsion of drops in an oscillating extensional flow," J. Non-Newtonian Fluid Mech. **128**, 71 (2005).
[21] X. Y. Li and K. Sarkar, "Effects of inertia on the rheology of a dilute emulsion of drops in shear," J. Rheol. **49**, 1377 (2005).
[22] X. Li and K. Sarkar, "Negative normal stress elasticity of emulsion of viscous drops at finite inertia," Phys. Rev. Lett. **95**, 256001 (2005).
[23] G. Subramanian and D. L. Koch, "Centrifugal forces alter streamline topology and greatly enhance the rate of heat and mass transfer from neutrally buoyant particles to a shear flow," Phys. Rev. Lett. **96**, 134503 (2006).
[24] G. Subramanian and D. L. Koch, "Inertial effects on the transfer of heat or mass from neutrally buoyant spheres in a steady linear velocity field," Phys. Fluids **18**, 073302 (2006).
[25] D. R. Mikulencak and J. F. Morris, "Stationary shear flow around fixed and free bodies at finite Reynolds number," J. Fluid Mech. **520**, 215 (2004).
[26] P. M. Kulkarni and J. F. Morris, "Pair-sphere trajectories in finite-Reynolds-number shear flow," J. Fluid Mech. **596**, 413 (2008).
[27] F. Pigeonneau and F. Feuillebois, "Collision of drops with inertia effects in strongly sheared linear flow fields," J. Fluid Mech. **455**, 359 (2002).
[28] J. M. Rallison, "The deformation of small viscous drops and bubbles in shear flows," Annu. Rev. Fluid Mech. **16**, 45 (1984).
[29] H. A. Stone, "Dynamics of drop deformation and breakup in viscous fluids," Annu. Rev. Fluid Mech. **26**, 65 (1994).
[30] E. Lac and D. Barthes-Biesel, "Pairwise interaction of capsules in simple shear flow: Three-dimensional effects," Phys. Fluids **20**, 040801 (2008).
[31] E. Lac, A. Morel, and D. Barthes-Biesel, "Hydrodynamic interaction between two identical capsules in simple shear flow," J. Fluid Mech. **573**, 149 (2007).
[32] S. O. Univerdi and G. Tryggvason, "A front-tracking method for viscous, incompressible, multi-fluid flows," J. Comput. Phys. **100**, 25 (1992).
[33] G. Tryggvason, B. Bunner, A. Esmaeeli, D. Juric, N. Al-Rawahi, W. Tauber, J. Han, S. Nas, and Y. J. Jan, "A front-tracking method for the computations of multiphase flow," J. Comput. Phys. **169**, 708 (2001).
[34] N. Aggarwal and K. Sarkar, "Deformation and breakup of a viscoelastic drop in a Newtonian matrix under steady shear," J. Fluid Mech. **584**, 1 (2007).
[35] X. Y. Li and K. Sarkar, "Front tracking simulation of deformation and buckling instability of a liquid capsule enclosed by an elastic membrane," J. Comput. Phys. **227**, 4998 (2008).
[36] M. Zurita-Gotor, J. Blawzdziewicz, and E. Wajnryb, "Swapping trajectories: A new wall-induced cross-streamline particle migration mechanism in a dilute suspension of spheres," J. Fluid Mech. **592**, 447 (2007).
[37] S. Guido and M. Simeone, "Binary collision of drops in simple shear flow by computer-assisted video optical microscopy," J. Fluid Mech. **357**, 1 (1998).
[38] G. I. Taylor, "The formation of emulsions in definable fields of flow," Proc. R. Soc. London, Ser. A **146**, 501 (1934).
[39] H. P. Grace, "Dispersion phenomena in high viscosity immiscible fluid systems and application of static mixers as dispersion devices in such systems," Chem. Eng. Commun. **14**, 225 (1982).
[40] G. Subramanian and J. F. Brady, "Trajectory analysis for non-Brownian inertial suspensions in simple shear flow," J. Fluid Mech. **559**, 151 (2006).